

ALMASOP. The Localized and Chemically rich Features near the Bases of the Protostellar Jet in HOPS 87

SHIH-YING HSU ¹, CHIN-FEI LEE ¹, SHENG-YUAN LIU ¹, DOUG JOHNSTONE ^{2,3}, TIE LIU ⁴, SATOKO TAKAHASHI ^{5,6},
LEONARDO BRONFMAN ⁷, HUEI-RU VIVIEN CHEN ⁸, SOMNATH DUTTA ¹, DAVID J. EDEN ⁹, NEAL J. EVANS II ¹⁰,
NAOMI HIRANO ¹, MIKA JUVELA ¹¹, YI-JEHNG KUAN ^{12,1}, WOJIN KWON ^{13,14}, CHANG WON LEE ^{15,16},
JEONG-EUN LEE ¹⁷, SHANGHUO LI ¹⁸, CHUN-FAN LIU ¹, XUNCHUAN LIU ¹⁹, QIUYI LUO ^{20,21,22}, SHENG-LI QIN ²³,
DIPEN SAHU ^{24,25}, PATRICIO SANHUEZA ^{5,6}, HSIEN SHANG (尚賢) ²⁶, KENICHI TATEMATSU ^{27,6} AND YAO-LUN YANG ²⁸

¹*Institute of Astronomy and Astrophysics, Academia Sinica, No.1, Sec. 4, Roosevelt Rd, Taipei 106216, Taiwan (R.O.C.)*

²*NRC Herzberg Astronomy and Astrophysics, 5071 West Saanich Rd, Victoria, BC, V9E 2E7, Canada*

³*Department of Physics and Astronomy, University of Victoria, Victoria, BC, V8P 5C2, Canada*

⁴*Key Laboratory for Research in Galaxies and Cosmology, Shanghai Astronomical Observatory, Chinese Academy of Sciences, 80 Nandan Road, Shanghai 200030, People's Republic of China*

⁵*National Astronomical Observatory of Japan, National Institutes of Natural Sciences, 2-21-1 Osawa, Mitaka, Tokyo 181-8588, Japan*

⁶*Department of Astronomical Science, The Graduate University for Advanced Studies, SOKENDAI, 2-21-1 Osawa, Mitaka, Tokyo 181-8588, Japan*

⁷*Departamento de Astronomía, Universidad de Chile, Casilla 36-D, Santiago, Chile*

⁸*Department of Physics and Institute of Astronomy, National Tsing Hua University, Hsinchu, 30013, Taiwan*

⁹*Armagh Observatory and Planetarium, College Hill, Armagh, BT61 9DB, UK*

¹⁰*Department of Astronomy, The University of Texas at Austin, 2515 Speedway, Stop C1400, Austin, Texas 78712-1205, USA*

¹¹*Department of Physics, P.O.Box 64, FI-00014, University of Helsinki, Finland*

¹²*Department of Earth Sciences, National Taiwan Normal University, Taipei, Taiwan (R.O.C.)*

¹³*Department of Earth Science Education, Seoul National University, 1 Gwanak-ro, Gwanak-gu, Seoul 08826, Republic of Korea*

¹⁴*SNU Astronomy Research Center, Seoul National University, 1 Gwanak-ro, Gwanak-gu, Seoul 08826, Republic of Korea*

¹⁵*Korea Astronomy and Space Science Institute (KASI), 776 Daedeokdae-ro, Yuseong-gu, Daejeon 34055, Republic of Korea*

¹⁶*University of Science and Technology, Korea (UST), 217 Gajeong-ro, Yuseong-gu, Daejeon 34113, Republic of Korea*

¹⁷*Department of Physics and Astronomy, Seoul National University, 1 Gwanak-ro, Gwanak-gu, Seoul 08826, Korea*

¹⁸*Max Planck Institute for Astronomy, Königstuhl 17, D-69117 Heidelberg, Germany*

¹⁹*Shanghai Astronomical Observatory, Chinese Academy of Sciences, Shanghai 200030, PR China*

²⁰*Shanghai Astronomical Observatory, Chinese Academy of Sciences, Shanghai 200030, People's Republic of China*

²¹*School of Astronomy and Space Sciences, University of Chinese Academy of Sciences, No. 19A Yuquan Road, Beijing 100049, People's Republic of China*

²²*Key Laboratory of Radio Astronomy and Technology, Chinese Academy of Sciences, A20 Datun Road, Chaoyang District, Beijing, 100101, P. R. China*

²³*Department of Astronomy, Yunnan University, and Key Laboratory of Astroparticle Physics of Yunnan Province, Kunming, 650091, People's Republic of China*

²⁴*Physical Research laboratory, Navrangpura, Ahmedabad, Gujarat 380009, India*

²⁵*Academia Sinica Institute of Astronomy and Astrophysics, 11F of AS/NTU Astronomy-Mathematics Building, No.1, Sec. 4, Roosevelt Rd, Taipei 106216, Taiwan, R.O.C.*

²⁶*Institute of Astronomy and Astrophysics, Academia Sinica, Taipei 106216, Taiwan*

²⁷*Nobeyama Radio Observatory, National Astronomical Observatory of Japan, National Institutes of Natural Sciences, 462-2 Nobeyama, Minamimaki, Minamisaku, Nagano 384-1305, Japan*

²⁸*Star and Planet Formation Laboratory, RIKEN Cluster for Pioneering Research, Wako, Saitama 351-0198, Japan*

Submitted to ApJ

ABSTRACT

HOPS 87 is a Class 0 protostellar core known to harbor an extremely young bipolar outflow and a hot corino. We report the discovery of localized, chemically rich regions near the bases of the two-lobe bipolar molecular outflow in HOPS 87 containing molecules such as H₂CO, ¹³CS, H₂S, OCS, and CH₃OH, the simplest complex organic molecule (COM). The locations and kinematics suggest that these localized features are due to jet-

driven shocks rather than being part of the hot corino region encasing the protostar. The COM compositions of the molecular gas in these jet-localized regions are relatively simpler than those in the hot corino zone. We speculate that this simplicity is due to either the liberation of ice with a less complex chemical history or the effects of shock chemistry. Our study highlights the dynamic interplay between the protostellar bipolar outflow, disk, inner core environment, and the surrounding medium, contributing to our understanding of molecular complexity in solar-like young stellar objects.

Keywords: astrochemistry — ISM: molecules — stars: formation and low-mass

1. INTRODUCTION

Interstellar complex organic molecules (COMs or iCOMs) found within low-mass young stellar objects (YSOs) are significant in astronomy due to their potential role in prebiotic chemistry in protoplanetary systems. The presence of warm gaseous COMs in YSOs is often explained by the “thermal desorption” paradigm (e.g., Garrod et al. 2007; Herbst & van Dishoeck 2009). Initially, during the starless core phase, with a temperature of ~ 10 K, CO molecules are primarily depleted by freeze-out and trapped in the icy mantles coating dust grains. Through grain-surface reactions, such as hydrogenation, COMs gradually form within these CO-rich ices. As the core evolves into the protostellar stage, the central protostar heats up the surrounding envelope, causing the desorption of these previously trapped COMs. In the innermost envelope, where temperatures exceed the ice sublimation threshold of ~ 100 K, the majority of the trapped COMs are released into the gas of the newly formed hot corino (Ceccarelli 2004). Hot corinos are commonly observed in protostellar cores, provided that their innermost envelopes attain temperatures of at least 100 K and guarantee ice sublimation (Ceccarelli 2004; Hsu et al. 2023). Furthermore, protostellar outbursts may extend the boundaries of thermal desorption due to the rapid increase of the temperature in the disk (Lee et al. 2019b).

In addition to the heating from the central protostar, shocks also play a role in releasing COMs in the gas phase. For example, COM factories have been discovered in the protostellar outflow L1157, particularly in the B1 shock region (e.g., Arce et al. 2008; Mendoza et al. 2014; Codella et al. 2015; Lefloch et al. 2017). Arce et al. (2008) suggested that COMs are primarily formed on the grain surfaces and then expelled from icy mantles by shocks. For [BHB2007] 11, a protobinary protostellar system, Vastel et al. (2022) suggested that the presence of hot methanol is due to shocks possibly generated by streamers towards the cores, impacting the quiescent gas within the circumbinary envelope, circumbinary disk, or the two circumstellar disks. Similarly, in the nearly edge-on protostellar disk around HH-212 (e.g., Codella et al. 2016; Lee et al. 2017, 2019a), some COMs near the disk edge may be released by the heat generated by “accretion shocks” (Lee et al. 2017; Tabone et al. 2017), while others away from the disk edge could be

released by the heat obtained from the radiation of the central protostar and/or disk-wind interaction (Lee et al. 2022). A similar accretion shock mechanism was proposed by Oya & Yamamoto (2020) based on the steep rise in H_2CS rotation temperature to 300 K or higher at a radius of 50 au from the protostar in IRAS 16293–2422 A. This localized heating mechanism received further support from the detection of an elevated ring-like warm structure in the Class 0 protostellar core B335 (Okoda et al. 2022).

These findings underscore the potential and significance of shocks in investigating COMs in YSOs, as they are potentially capable of releasing COMs from the ice phase to the gas phase. Furthermore, chemically rich shocked regions may exhibit distinct chemical characteristics compared to hot corinos where the ice is more gradually sublimated. For instance, certain COMs such as CH_3CHO are observed to be more prevalent in the L1175-B1 shocked region than in hot corinos, with abundance ratios ranging from 2 to 10, depending on the species (Lefloch et al. 2017). Additionally, some studies suggest that gas-phase reactions are enhanced following shocks (Codella et al. 2015). The limited identification of chemically rich shocked regions leads to a desire for further discoveries and in-depth investigations, particularly targeting those YSOs hosting abundant COMs.

HOPS 87 (Furlan et al. 2016), also known as OMC-3 MMS 6 (Chini et al. 1997) and G208.68-19.20N1 (Dutta et al. 2020), is a Class 0 protostellar core in the Orion Molecular Cloud 3 (OMC-3) region with a bolometric luminosity L_{bol} of $38 \pm 13 L_{\odot}$, a bolometric temperature T_{bol} of 36.7 ± 14.5 K, and local standard of rest velocity v_{LSR} of 11.4 km s^{-1} (Dutta et al. 2020). This source is one of the 11 protostellar cores with a detected hot corino reported by the “ALMA Survey of Orion PGCCs (ALMASOP)” project (Hsu et al. 2020, 2022), where the ALMA is Atacama Large Millimeter/submillimeter Array and the PGCCs are Planck Galactic Cold Clumps (Planck et al. 2016). It is the third-most luminous protostellar core in the catalogued sample. There are several COM species detected toward this source, including CH_3OH , CH_2DOH , $^{13}\text{CH}_3\text{OH}$, CH_3CHO , HCOOCH_3 , and NH_2CHO .

Takahashi & Ho (2012) reported an extremely young outflow associated with HOPS 87 (MMS6) with an estimated outflow dynamic range of ≤ 100 yr. The authors reported an

inclination of 45° for the bipolar outflow by comparing their position-velocity (PV) diagram with a kinetic outflow model (Lee et al. 2000). Takahashi et al. (2019) later estimated the inclination angle to be 60° (roughly edge-on) based on comparisons between the observed toroidal magnetic field and numerical calculations. Takahashi & Ho (2012) reported a detection of HCN ($J = 4 - 3$), tracing an increase in line width at the end of the molecular outflow, which indicates a clear bow-shock type velocity structure. The jets in HOPS 87 were recently studied by Dutta et al. (2024), and the projected velocity of the jets was reported to be $43 \pm 6 \text{ km s}^{-1}$. Assuming that the majority of low-velocity components in the bipolar outflow are wind components, the authors estimated an inclination angle of the bipolar outflow to be 65° .

In this paper, we report newly discovered, localized, chemically rich regions associated with jet-driven shocks near the two bases of the bipolar outflow in the protostellar core HOPS 87. In §2, we introduce the two observation programs used for this study. In §3.1, we show the (integrated) intensity maps of selected molecular transitions, which reveal the two-lobe, localized, and chemically rich regions near the bases of the bipolar molecular outflow. Moreover, in §3.2, we investigate the kinematics in the localized regions. In §4 and §5, we discuss our findings and make summarize our conclusions, respectively.

2. OBSERVATIONS

This study mainly retrieves data obtained from the ALMASOP program (#2018.1.00302.S) and supplemental data obtained from an earlier archival ALMA project (#2015.1.00341.S).

2.1. ALMASOP Project: ALMA Cycle 6 #2018.1.00302.S

The ALMASOP data were obtained from ALMA Cycle 6 program #2018.1.00302.S (PI: Tie Liu) in Band 6 (1.3 mm or 230 GHz) with the combination of both the 12-m array (configurations C43–5 and C43–2) and 7-m array (also known as Atacama Compact Array, ACA, or Morita Array). The projected baselines ranged from 4.7 to 1066 k λ , and the resulting maximum recoverable scale was approximately $26''$. This survey selected 72 clumps in the Orion A, B, and λ Orionis clouds as targets, beginning from a sample of PGCCs (Planck et al. 2016). The four spectral windows centered at 216.6, 218.9, 231.0, and 233.0 GHz have a uniform bandwidth of 1,875 MHz with a spectral resolution of 1.129 MHz (1.4 km s^{-1} at 230 GHz).

We used `tclean` in CASA (CASA Team et al. 2022) with a robust value of 2.0. The resulting angular resolution was $\sim 0''.42$ (which corresponds to about 168 au for a distance of $\sim 400 \text{ pc}$) for both continuum and continuum-subtracted data cubes, and the sensitivities of the image reach

$\sim 12 \mu\text{Jy beam}^{-1}$ and $\sim 3.3 \text{ mJy beam}^{-1}$ for the full-band continuum and each channel, respectively. For more details about the ALMASOP project, please refer to Dutta et al. (2020).

2.2. Archival Data: ALMA Cycle 3 #2015.1.00341.S

This study also retrieved ALMA Band 6 data obtained from a Cycle 3 program (#2015.1.00341.S, PI: Satoko Takahashi) for better-visualizing the intensity maps of the CO $2 - 1$ and CH₃OH $5_{1,4} - 4_{2,4}$ transitions as it had a much better spatial resolution (FWHM beam size $\sim 0''.16$). These observations were conducted on 2016 September 18. The data cubes used in this study have a spectral resolution of 0.244 MHz, corresponding to a velocity resolution of 0.32 km s^{-1} . The projected baseline ranged from 16 to 3200 k λ , and the maximum recoverable scale was about $1''$.

The images exported by the Additional Representative Images for Legacy (ARI-L) project (Massardi et al. 2021) were utilized. ARI-L, endorsed by the Joint ALMA Observatory (JAO) and the European Southern Observatory (ESO), is a European Development project for ALMA. Its primary objective is to employ the ALMA Imaging Pipeline on data from initial observing cycles (2–4) to regenerate data products with equivalent completeness and quality to those currently produced by ALMA for recent observations. The original CASA pipeline version was 4.7.0 and the Briggs robust parameter was set to 0.5. With a FWHM beam size of $0''.16$, the sensitivity achieved $\sim 6 \text{ mJy beam}^{-1}$ for a channel width of 0.244 MHz.

3. RESULTS

3.1. Dust Continuum and Molecular Line Emission

Table A1 lists the information of the molecular transitions used in this study. Figure 1 shows the integrated intensity images of selected molecular transitions within a size of $4''.0$ ($\sim 1600 \text{ au}$) overlaid by 1.3 mm continuum and the SiO integrated intensity maps. For completeness, the integrated intensity images of all the molecular transitions in this study are shown in Figure A1.

3.1.1. 1.3 mm Dust Continuum

Figure 1 shows the observed 1.3 mm dust continuum which appears to trace the extended envelope. As illustrated by the dashed black contours, the continuum is spherically-symmetric at the small scale ($\sim 150 \text{ au}$), becomes elongated at a middle scale ($\sim 400 \text{ au}$), and extend to north and east at a large scale ($\sim 600 \text{ au}$). The brightness temperature of the 1.3 mm continuum peak is 47 K with a beam size of $0''.42$. Takahashi et al. (2012) and Takahashi et al. (2019) reported brightness temperatures of 52 K and 192 K with beam sizes of $0''.27$ and $0''.024$, respectively. These relatively high dust continuum brightness temperatures suggest that the inner

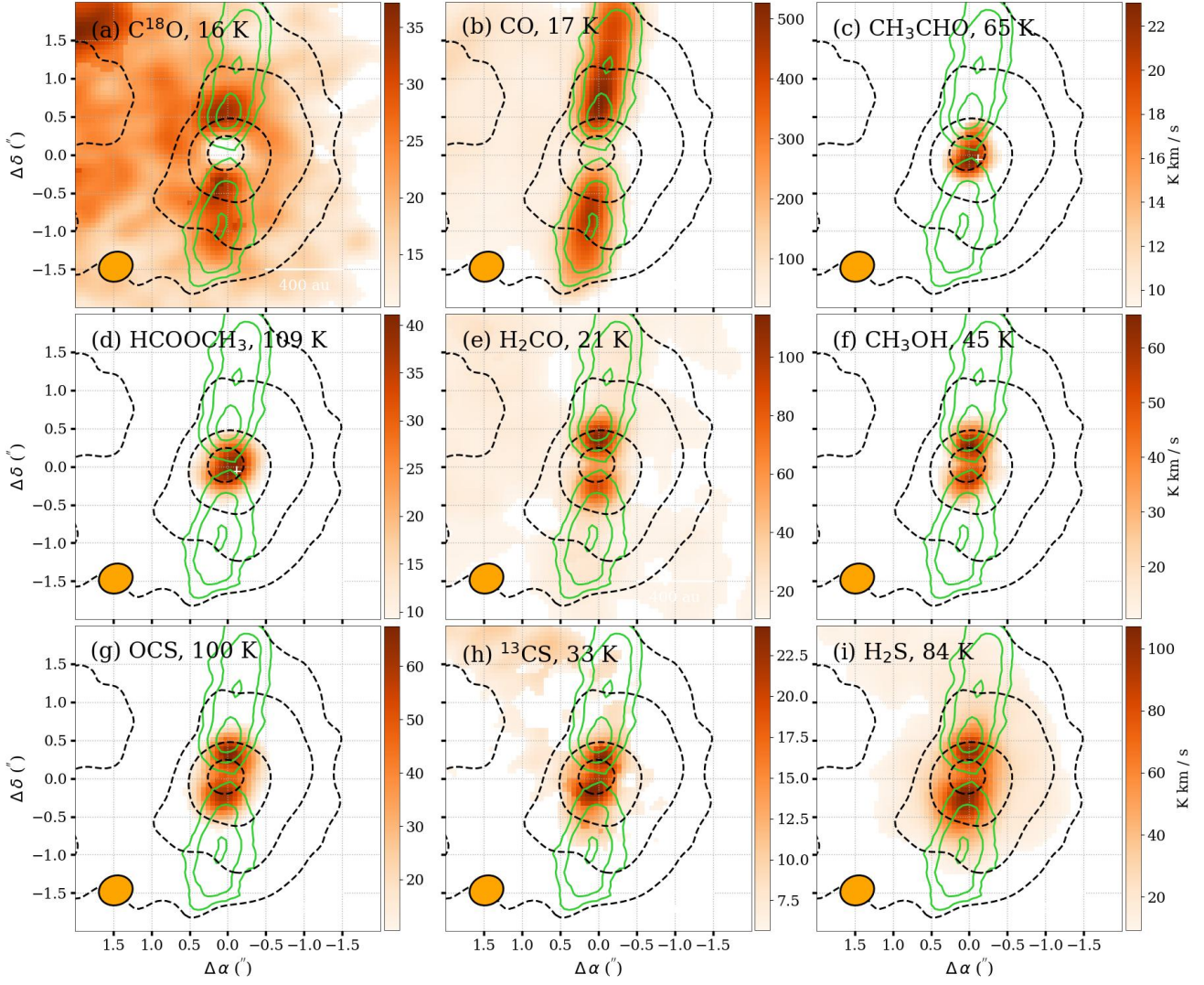


Figure 1. Integrated intensity images (moment-0 maps) of selected molecular transitions: C^{18}O , CO , CH_3CHO , HCOOCH_3 , H_2CO , CH_3OH , OCS , ^{13}CS , and H_2S . The origin of the coordinate system is the 1.3 mm continuum peak at $[\alpha_{2000}, \delta_{2000}] = [05^{\text{h}}35^{\text{m}}23^{\text{s}}.42, -05^{\circ}01'30''.6]$, and the ranges of right ascension (x-axis) and declination (y-axis) span $\pm 2''$. Each panel is labeled at the top with the corresponding chemical formula and the upper energy level of the transition shown in color. The velocity ranges for integration are $\pm 40 \text{ km s}^{-1}$ for CO and SiO , $\pm 3 \text{ km s}^{-1}$ for ^{13}CS , and $\pm 7.5 \text{ km s}^{-1}$ for others. The black dashed contours depict the 1.3 mm continuum, set at levels of $[5, 10, 20, 40, 80, 160]\sigma$, where σ corresponds to $0.9 \text{ mJy beam}^{-1}$ (or 0.13 K in terms of brightness temperature). The orange ellipse located at the bottom left corner indicate the beam sizes for the Cycle 6 ALMA program. The green contours display the SiO integrated intensity map, highlighted at levels of $[10, 25, 40]\sigma$, where each σ corresponds to $28 \text{ mJy beam}^{-1} \text{ km s}^{-1}$. The distribution of the molecules in panels (e)–(i) are particularly noteworthy; these molecules are not typical outflow tracers but exhibit two-lobed distributions. The white cross in panels (c) and (d) illustrate the peak position of the corresponding transition.

region is very warm, similar with the cases of NGC 1333 IRAS 4A1 (57 K) and 4A2 (42 K) reported by Sahu et al. (2019). In addition, HOPS 87 and IRAS 4A2 are reported to harbor hot corinos (e.g., Hsu et al. 2022; Sahu et al. 2019). Due to these similarities, we adopt the assumed dust temperature (60 K) from Sahu et al. (2019) for evaluating the optical depth and the molecular hydrogen column density. We note that the beam size of our study ($\sim 160 \text{ au}$) is larger than the value ($\sim 80 \text{ au}$) of Sahu et al. (2019). As a result, this adopted continuum brightness temperature (60 K) could

be overestimated. In such case, the derived optical depth and the molecular hydrogen column density in the following contexts are their lower limits.

We evaluate the optical depth (τ_ν) using the following equation adopted from Kauffmann et al. (2008):

$$I_\nu = B_\nu(T_d)(1 - e^{-\tau_\nu}) = \frac{F_\nu^{\text{beam}}}{\Omega_A}, \quad (1)$$

where I_ν is the beam-averaged intensity, B_ν is the Planck function, T_d is the dust temperature, F_ν^{beam} is the observed

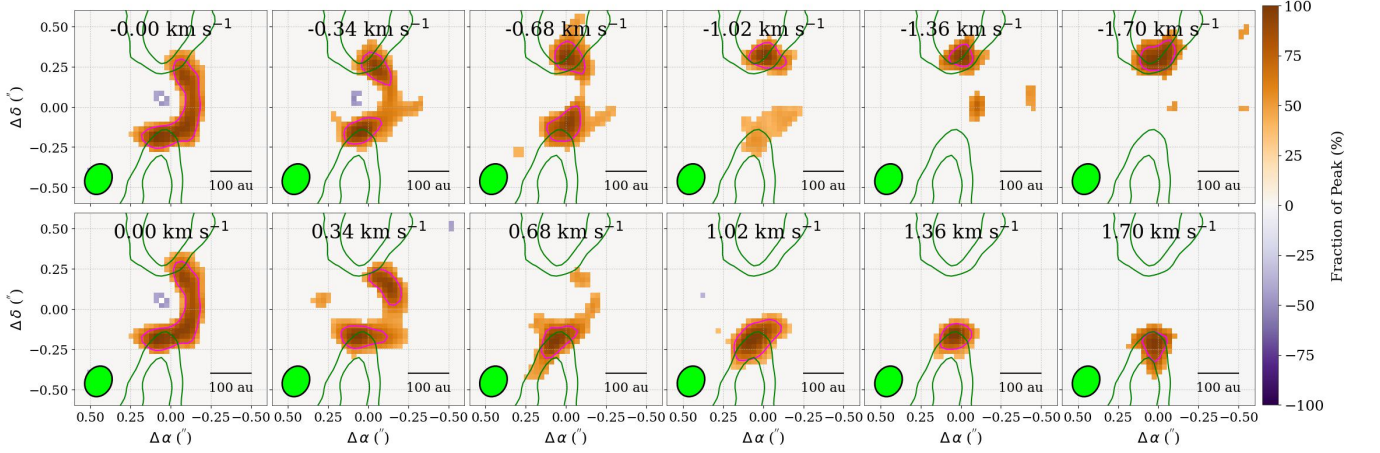


Figure 2. The $\text{CH}_3\text{OH } 5_{1,4} - 4_{2,3}$ transition in Cycle 3 observations. The top and bottom rows show the images at the blue- and red-shifted channels, respectively. The labels in each panel shows the relative velocity ($\Delta v = v - v_{\text{LSR}}$). At $\Delta v = 0 \text{ km s}^{-1}$ the intensity map displays an arc-like emission pattern west of the center with an absorption feature toward the continuum peak. At $|\Delta v| > 0.68 \text{ km s}^{-1}$, there is a single lobe ($\Delta\delta \sim 0''.3$) on each of the northern and the southern sides of the arc ($\Delta\delta \sim 0''.2$) seen at $\Delta v = 0 \text{ km s}^{-1}$.

flux per beam, and Ω_A is the solid angle of the beam. Adopting the brightness temperature at the continuum peak, the derived optical depth τ_ν is 1.55, indicating that the continuum is somewhat optically thick.

We estimate the molecular hydrogen column density $N(\text{H}_2)$ adopting Equation A.9 in Kauffmann et al. (2008):

$$N(\text{H}_2) = \frac{\tau_\nu}{\mu m_{\text{H}} \kappa_\nu}, \quad (2)$$

where μ is the molecular weight per hydrogen molecule ~ 2.8 , m_{H} is the mass of atomic hydrogen, and κ_ν is the dust mass opacity. To estimate κ_ν , we adopt the form of $\kappa_\nu = 0.1(\nu/\text{THz})^\beta \text{ cm}^2 \text{ g}^{-1}$, where β is the dust opacity index, from Beckwith et al. (1990). We assume the index β to be 1.70, which is the typical opacity index of cold clumps in the submillimeter band (Juvella et al. 2018), and the estimated κ_ν is $0.0083 \text{ cm}^2 \text{ g}^{-1}$ at 1.3 mm. Assuming a gas-to-dust ratio of 100, the resulting molecular hydrogen column density $N(\text{H}_2)$ is $2.89 \times 10^{25} \text{ cm}^{-2}$.

3.1.2. C^{18}O : Extended Warm Gas

C^{18}O is a good tracer of warm gas, as it is released into gas phase at a temperature of $\sim 20 \text{ K}$ (Tychoniec et al. 2021) and has a low critical density ($\sim 10^4 \text{ cm}^{-3}$ for $J = 2 - 1$, Saito et al. 2001). We show in Figure 1 (a) the C^{18}O integrated intensity map, which overall extends to the north and east, is consistent with the dust continuum. In addition to the extended gas, there appears to be a hole absent of emission centered at the continuum peak position with a size of $0''.5$, which is comparable to the beam size. Given that the C^{18}O emission is significant around the hole, it is unlikely that it results from a complete absence of C^{18}O molecules. This hole could be due to the comparable dust (continuum) temperature and the C^{18}O gas (excitation) temperature.

At the north and south sides of the hole, the bright C^{18}O emission may result from the bipolar outflow, as the positions are corresponding to the outflow lobes illustrated by the green contours. Near the northeast corner ($\Delta\alpha \sim +1''.5$, $\Delta\delta \sim +1''.5$) of panel (a), a separated peak of C^{18}O integrated intensity is detected and corresponds to a separate source (MMS6-NE at 0.9 mm and IRS 3 at near-IR) identified as a Class I protostellar core by Takahashi et al. (2009).

3.1.3. CO and SiO : Outflows

We show in Figure 1 (b) the integrated intensity map of the typical outflow tracer $\text{CO } (J = 2 - 1)$. Consistent with the discoveries of Takahashi & Ho (2012) in $\text{CO } (3 - 2)$, the bipolar outflow, which is compact (about $2''$ long for each lobe), exhibits two lobes at the northern and southern sides. As we will show in the following sections, the blue-shifted and red-shifted characteristics are in the northern and southern lobes, respectively. The absence of CO emission at the region below a Δp (the position offset from the continuum peak position) of $0''.2$ is due to both absorption along the line of sight and missing flux at low velocities due to interferometry. For the former, the absorption feature is also confirmed in the line profile at the continuum peak position. The latter was anticipated as implied from the PV diagram shown in Sect. 3.2.

SiO is another well-known outflow gas tracer, particularly the protostellar jet and the consequent shocked and collision regions. As illustrated by the green contours in Figure 1, SiO also trace outflowing gas in HOPS 87. The sizes of the northern and southern SiO lobes are comparable to those of the CO outflows.

3.1.4. CH_3CHO and HCOOCH_3 : Hot Corino Zone

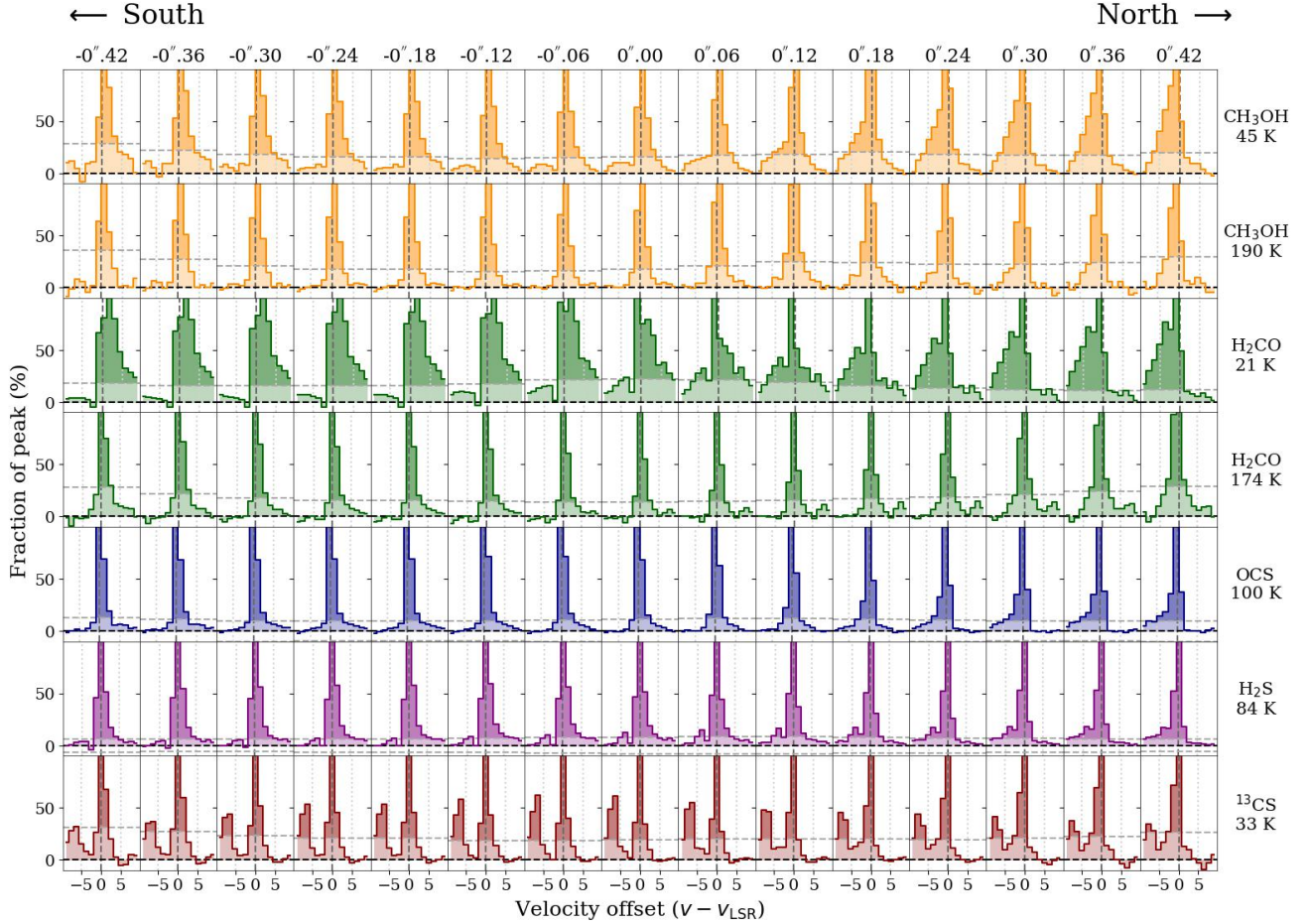


Figure 3. Spectra of selected molecular transitions along the cavity axis. The labels at the right of each row show the formula and the upper energy of each transition. The labels at the top of each column show the angular offset from the continuum peak. The horizontal dashed lines represent the level of 5σ . In the panels of ^{13}CS , the lines at $\sim -7 \text{ km s}^{-1}$ is another molecular transition. The y-axis is the fraction of peak intensity. The north is blue-shifted (coming toward us) and the south is red-shifted (moving away), and the lines extend to bluer and redder velocities at the north and south positions, respectively.

A hot corino is a warm region, particularly the innermost envelope (Hsu et al. 2023) around a low-mass protostar, abundant in saturated COMs such as CH_3CHO and HCOOCH_3 . Figure 1 (c) and (d) show the CH_3CHO 65 K and HCOOCH_3 109 K integrated intensity images, respectively, which illustrate the compact hot corino zone previously reported by Hsu et al. (2020) and Hsu et al. (2022). This hot corino zone resides in the hole seen in the C^{18}O map, supporting that the hole seen in the C^{18}O integrated intensity map likely does not result from a lack of C^{18}O gas.

As illustrated by the white crosses in Figure 1 (c) and (d), the bright COM emission is slightly offset toward the west from the continuum peak position. Figure 2 shows the intensity maps at each channel of a CH_3OH transition obtained from the Cycle 3 observations At $\Delta v = 0 \text{ km s}^{-1}$ the intensity map displays an arc-like emission pattern west of the center with an absorption feature toward the continuum peak. This arc outlines where the hot corino is, which is

the warm COM emission resided in the innermost envelope, where the C^{18}O emission shows the absorption feature. The existing COM emission also suggest that the temperatures of the COMs are higher than that of C^{18}O . In other words, the warm gas-phase COM molecules are distributed in both the central absorption region and the arc emission region, and the former is due to the even hotter continuum at the center. As a result, the offset of the COM emission observed in our Cycle 6 program results from the asymmetric innermost warm envelope gas surrounding the central warmer continuum optically thick region. It is noteworthy that the distribution is different at higher velocities, which will be elaborated on in the following sections. The COM absorption feature we observed in CH_3OH is also been seen in IRAS 4A1 (Sahu et al. 2019) and IRAS 16293-2422 B (e.g., Oya et al. 2018).

3.1.5. Molecules Exhibiting Two Localized Lobes

In Figure 1, some molecules, namely H_2CO (panel e), OCS (panel g), ^{13}CS (panel h), and H_2S (i), apparently

exhibit two-lobe signatures. Interestingly, CH_3OH (panel f) exhibits a two-lobe signature in addition to its hot corino localization at low velocities. These molecules are not “typical” outflow tracers, while H_2CO could also trace the low-velocity outflows (Izumi et al. 2024). The position offset from the continuum peak (Δp) of the lobes for different molecules are similar ($\sim 0''.3$), indicating that the two regions are chemically rich. The sizes of the lobes are comparable to the size of the beam, indicating that these chemically rich regions are localized.

These two chemically rich localized regions are near the bases of the bipolar SiO molecular outflow (green contours). We first checked whether the two regions are the outer extended parts of the hot corino in HOPS 87. As shown in Figure 2, the intensity maps at $\Delta v = 0 \text{ km s}^{-1}$ and at $|\Delta v| > 0.68 \text{ km s}^{-1}$ display different patterns. The former traces the hot corino zone, as we discuss in Sect. 3.1.4, whereas the latter exhibits a single lobe on each of the northern and the southern sides of the hot corino zone. Particularly at $|\Delta v| < 0.68 \text{ km s}^{-1}$, the position offset of the lobe ($\Delta\delta \sim 0''.3$) appears to be slightly beyond the “boundary” of the hot corino ($\Delta\delta \sim 0''.2$) seen at $\Delta v = 0 \text{ km s}^{-1}$. These observations suggest that the two lobes and the hot corino are tracing different regions. Moreover, the positions of the lobes, along with their consistent velocity directions with the bipolar outflow imply the potential association of the molecular gas with the bipolar outflow. This could be similar to OCS in the high-mass protostellar core NGC 2264 CMM3B, which also exhibits two lobes at the bases of the outflows, as found by Shibayama et al. (2021). The authors suggest that the OCS is tracing the bases of outflows in addition to the disk/envelope system.

3.2. Kinematics

To further justify the association between the bipolar outflow and the two localized chemically rich regions, we initially extract the continuum-subtracted spectra along the cavity axis (position angle $\text{PA} = -4^\circ$), centered at the 1.3 mm continuum peak. Figure 3 depicts the spectra of selected molecular transitions along the outflow axis. Note that the y-axis is the fraction of peak intensity for better visualizing the line profiles of all pixels. Despite the limited spectral resolution ($\sim 1.3 \text{ km s}^{-1}$), discernible symmetry between spectra at the north and south positions is observed. Firstly, the north is blue-shifted, coming toward us, and the south is red-shifted, moving away. Secondly, the lines extend to bluer and redder velocities at the north and south positions, respectively. These consistencies solidify their associations with the bipolar outflow. The velocity of the CO outflow reaches 40 km s^{-1} (Dutta et al. 2020), while the velocities of the molecules in Figure 3 are around 5 km s^{-1} .

To have a closer look at the kinematics, we made the position-velocity (PV) diagrams (Figure 4) cut along the outflow axis with an average width of three pixels with a pixel size of $0''.06$ using CARTA 4.0 (Comrie et al. 2021). First, the gap of the CO (grey contours) at $\Delta v = 0 \text{ km s}^{-1}$ indicates the missing flux due to interferometry at low velocities. Second, as shown in Figure 4 (k), the rapid growth of velocity Δv with position offset Δp from $\Delta p = 0''$ to $0''.3$ and $-0''.2$ is significant in SiO. Finally, as shown in Figure 4 (a) to (g), the broadening of the velocity range localized at $\Delta p = 0''.3$ and $-0''.2$ is significant in CH_3OH , H_2CO , OCS, and H_2S and tentative in ^{13}CS . These characteristics suggest that these molecules (i.e., SiO, CH_3OH , H_2CO , OCS, H_2S , and ^{13}CS) are more likely tracing jet-driven outflows rather than wide-angle winds (Lee et al. 2001).

For the molecular transitions exhibiting two localized blobs, the northern ($\Delta p > 0''$) blobs have a larger velocity width than what the southern ($\Delta p < 0''$) blobs. As shown by the navy dashed polylines, most of the molecules including CH_3OH , OCS, and H_2S have comparable position offsets, indicating their possible common origin. The only exception is H_2CO , which has slightly higher position offset of $\sim 0''.40$. Finally, for all transitions, the position offsets of the northern blobs ($\Delta p \sim 0''.3$) are generally higher than the southern blobs ($-0''.2$), as also illustrated in Figure 2.

Figure 5 shows the velocity widths of the blobs, which is defined as the maximum speed for each lobe in the PV diagrams (Figure 4) filtered out by a threshold of 5σ . The velocity widths seem to be anti-correlated with upper energies of the molecular transitions observed. As illustrated in Figure 5, the velocity width of CH_3OH decreases from 5.6 km s^{-1} at $E_{\text{u}} = 45 \text{ K}$ to 2.8 km s^{-1} at $E_{\text{u}} = 190 \text{ K}$. For H_2CO , from the lowest ($E_{\text{u}} = 21 \text{ K}$) to the highest upper energy ($E_{\text{u}} = 174 \text{ K}$) transitions, the velocity width decreases from 9.8 to 2.8 km s^{-1} . These negative correlations could simply result from the different line intensities of the transitions having different upper energies, or it could possibly be due to the warmer gas at the inner regions. We favor the former based on the flat ratios between high and low transitions at high-velocity wings in Figure B1. In another word, the flat ratios imply that there is no significant change in the gas temperature. However, the weak line intensities at high velocity, particularly for the high-upper-energy transitions, prevent us from justifying this.

4. DISCUSSION

4.1. The Localized Chemically rich Features in HOPS 87

Our findings suggest that the two chemically rich regions localized near the bases of the molecular jet are due to jet-driven outflows. The hosting molecular inventories in the

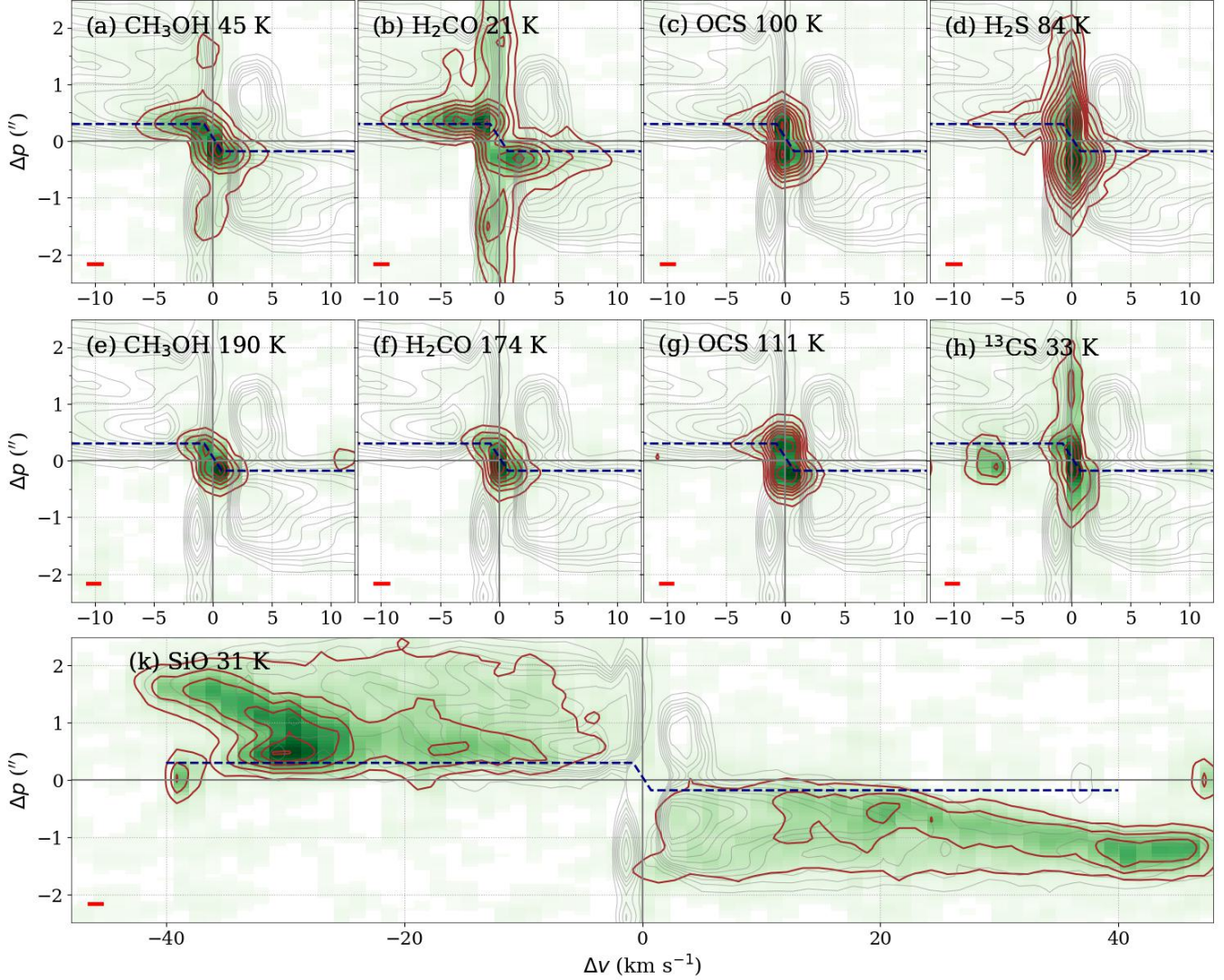


Figure 4. The PV diagrams of selected molecular transitions along the outflow axis (position angle $PA = -4^\circ$ with the center is at the 1.3 mm continuum peak). The relative position offset (Δp) is from south ($\Delta p < 0''$) to north ($\Delta p > 0''$). The upper left label in each panel show the chemical species and the upper energy E_u of the transitions. Note that the diagrams are exported from the data cube of the full spectral window so the separated components may come from molecular transitions other than the labeled one in each label (e.g., the components at $(-7.5 \text{ km s}^{-1}, 0'')$ in panel (h) and at $(-7.5 \text{ km s}^{-1}, 0'')$ in panel (k)). The color maps and the brown contours are the PV diagram of the labeled transitions. The grey contours represent the CO PV diagram. The brown and grey contours are in steps of $[5, 10, 15, 20, 25, 30, 40, 50, 60, 70, 80]\sigma$. The navy polyline, referred from the PV diagram of the CH_3OH 45 K transition, consists of two horizontal lines at $\Delta p = 0.3''$ and $-0.2''$ and a diagonal line moves from $\Delta p = 0.3''$ to $-0.2''$ at $\Delta v = 0.75 \text{ km s}^{-1}$ and -0.75 km s^{-1} , respectively. The diagrams are exported by CARTA 4.0 (Comrie et al. 2021). The gap in CO indicates the missing flux at low velocities due to interferometry. The broadening of the velocity range localized at $\Delta p = 0.3''$ and $-0.2''$ is significant in CH_3OH , H_2CO , OCS , and H_2S and tentatively observed in ^{13}CS . Additionally, the rapid growth of velocity Δv with position offset Δp described in Lee et al. (2001) is significant in SiO. These characteristics suggest that these molecules are also tracing jet-driven bow shocks (Lee et al. 2001).

shocked regions comprise H_2CO , CH_3OH , OCS , ^{13}CS , and H_2S .

Finally, for all transitions, the position offsets of the northern blobs ($\Delta p \sim 0.3''$) are generally higher than the southern blobs ($-0.2''$), as also illustrated in Figure 2. **Overall, most of the molecules have similar position offsets with each other for the northern lobe and the southern lobe individually. The only exception is**

H_2CO , which peaks at a slightly greater position offset. Meanwhile, the northern (blue-shifted) lobe peaks at a larger position offset than the south (red-shifted) lobe for both H_2CO and all other transitions.

4.1.1. The Origin of the Localized Chemically Rich Feature

Two potential mechanisms are proposed for the bringing COMs from the ice phase to the gas phase in YSOs:

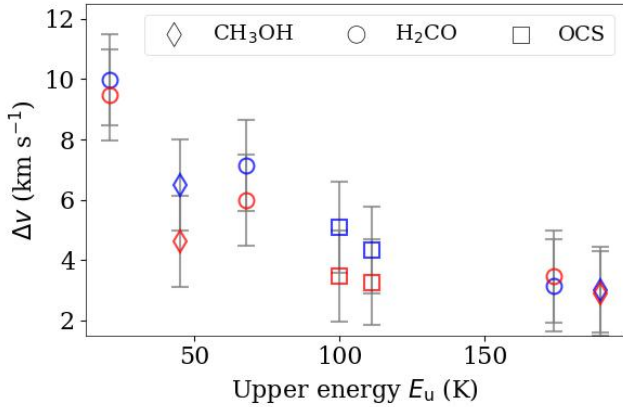


Figure 5. The velocity width versus upper energy for the molecular transitions in the two chemically rich regions. Only molecular species having multiple transitions are included. The blue and red markers represent the measurement at the blue-shifted (northern) and red-shifted (southern) lobes, respectively. The error bars are referred from the spectral channel widths ($\sim 1.4 \text{ km s}^{-1}$). The velocity width seem to be anti-correlated with upper energies of the molecular transitions, possibly due to the different populations of each transition state.

thermal desorption and grain sputtering. For the former, ice sublimates at approximately 100 K and the frozen molecules are exclusively released into the gas phase (e.g., Busch et al. 2022). In such case, the rotational temperature of the desorbed molecules is expected to be higher or comparable to the ice sublimation temperature at around 100 K. Even below ice sublimation temperature at $\sim 20\text{--}30 \text{ K}$, “partial” thermal desorption may possibly occur, specifically at the outermost layer of the icy mantle. This may result from lower binding energies (and consequently desorption energies), but the uncertain nature of these binding energies makes confirmation difficult (Busch et al. 2022). As discussed by Busch et al. (2022), partial thermal desorption is inefficient compared to the complete thermal desorption (i.e., co-evaporation with ice).

For the latter, the sputtering of grains requires shocks, commonly occurring when ejected/outflowing materials collide with the dense surrounding medium at high speeds. The collisions can release H_2O as well as COMs from the ice phase to the gas phase (e.g., Caselli et al. 1997; Jiménez-Serra et al. 2008). The velocity dispersion of the molecular lines is expected to be broad due to the nature of shocks. Shocks can also heat up the materials, leading to the thermal desorption of molecules (e.g., Miura et al. 2017). After the shock front, the shocked materials begin to cool and are not necessarily warm (e.g., James et al. 2020).

Among the above two mechanisms (i.e., ice sublimation and grain sputtering) able to lead the richness of molecules, in particular those form within ice mantle such as CH_3OH and OCS , our findings favor the shock-induced grain

sputtering picture due to (1) the velocity spur structures (i.e., wide velocity dispersion) of the molecular tracers and (2) the coexistence of SiO gas, an indicator of dust destruction (e.g., Guillet et al. 2009). Although we do not see the knots of the typical tracers, CO and SiO , at the same position offset, we do see SiO knots at slightly higher position offsets ($\Delta p = \pm 0''.5$), as shown in Figure 4 (k). We note that Le Gouellec et al. (2024) has detected molecular hydrogen lines in the $2 \mu\text{m}$ band in HOPS 87, a spectral feature typically associated with shocks in protostellar outflow cavities.

4.1.2. Comparisons with the counterpart hot corino

To compare the chemical compositions of the hot corino and chemically rich shocked regions near the outflow origins, we extracted the PV diagrams with cuts along and across the outflow axis for molecules tracing between jet (SiO), hot corino zone (HCOOCH_3 and CH_3OCH_3), and both regions (CH_3OH and H_2CO) in Figure 6. Note that the x-axes are in terms of frequency to cover multiple molecular transitions within each panel. As shown in 4 (a) and (b), the typical outflowing gas tracer SiO only appears in the cut along the outflow axis and shows a spur structure. In 4 (c) and (d), COMs HCOOCH_3 and CH_3OCH_3 exhibit a single peak in both diagrams, suggesting that they are present only in the hot corino zone. In contrast, as illustrated in 4 (e) and (f), CH_3OH and H_2CO show a single peak on the cut across the outflow axis and a spur signature on the cut along the outflow axis. This indicates that some molecules (i.e., CH_3OH and H_2CO) residing in the hot corino zone are also present in the shocked regions.

4.1.3. Implications

On the basis that COMs are thought to be primarily formed within the icy mantle on dust grains and then released into the gas phase (e.g., Herbst & van Dishoeck 2009; Yamamoto 2016), the observed gaseous COMs can reveal a glimpse of the ice composition. Therefore, the difference in gaseous COM composition between the hot corino zone and the jet-localized shocked regions in HOPS 87 suggests distinct ice compositions of the dust grains in these areas. In the hot corino zone of HOPS 87, the dust grains have hosted a variety of COMs such as CH_3CHO , HCOOCH_3 , and CH_3OCH_3 . The presence of these larger COMs (compared to CH_3OH) indicates that the ice mantles have had a prolonged period for complex chemistry to occur. In contrast, in the jet-localized shocked regions, the only firmly detected COM is CH_3OH . As the simplest COM and a precursor to larger COMs, the formation history of CH_3OH is relatively straightforward compared to larger COMs such as CH_3CHO . The formation of the former can be achieved via a series of hydrogenation with the frozen CO , and the formation of the latter requires more atoms/molecules as reactants (e.g., Herbst & van Dishoeck 2009; Yamamoto

2016). This suggests that either the icy mantle, at least its top layer, on dust grains in the shocked region have not undergone as extensive chemical processing, or they have experienced cycles of ice sublimation and reformation, limiting the formation of larger COMs.

Alternatively, the chemical composition could be affected by shocks. First, molecules could be destroyed by shocks (e.g., Holdship et al. 2017). For example, as speculated by Arce et al. (2008), the low $\text{CH}_3\text{CN}/\text{CH}_3\text{OH}$ ratio in L1157 B1 shock may be due to the rapid destruction of CH_3CN . Similarly, in HOPS 87, the larger COMs in the jet-localized regions could possibly be destroyed. Second, shocks may enhance chemical reactions not commonly present in cold gas through the so-called “shock chemistry,” due to factors such as high temperature and sputtered molecular species (e.g., Caselli et al. 1997; Burkhardt et al. 2019). As proposed by Codella et al. (2015), a significant fraction of CH_3CHO in L1157 B1 could form in the gas phase due to the shocks. Meanwhile, the chemical composition could be sensitive to the evolution of shocks and further serve as a probe of the shock stage (e.g., Burkhardt et al. 2016, 2019). A more comprehensive investigation of the physical parameters (e.g., temperature) would help constrain the shock models. This would further improve our understanding of the dynamic interplay between the protostellar bipolar outflow, disk, inner core environment, and the surrounding medium (e.g., Shu et al. 1996; Shang et al. 2023).

4.1.4. Comparison with L1157-B1

L1157-B1 is a jet-driven bow shock recognized for housing an inventory of COMs (e.g., Arce et al. 2008; Mendoza et al. 2014; Codella et al. 2015; Lefloch et al. 2017; Feng et al. 2020; Spezzano et al. 2020; Benedettini et al. 2021). Arce et al. (2008) estimated the timescale of the outflows to be roughly less than 2000 years, which is too short for their detected COMs to have formed primarily through gas-phase reactions. Additionally, the shock is far from the associated central protostar (spatial offset = $68''3$, distance = 250 pc), rendering thermal desorption due to the central protostar unlikely. The authors concluded that the COMs more likely formed on the grain surface and then were expelled from the icy mantles by the shock.

For HOPS 87, we expect that the temperature of the molecules residing in the two jet-localized regions are warm based on the detection of transition having high upper energies (e.g., OCS 100 and 111 K transitions.) In contrast, the rotational temperatures of molecules within the L1157-B1 shock typically range from 20 to 50 K. For instance, the kinematic temperature of OCS was reported to be 46.8 ± 3.4 K by Holdship et al. (2019). As demonstrated by Busquet et al. (2017), this relatively low temperature may possibly be a result of cooling after the shocks. On the basis

of their demonstration, the relatively warm shocked region in HOPS 87 suggests that the cooling process is insignificant, consistent with the reported short dynamic age of the outflow.

4.2. Suspected Component at the Bow Shocks

In Figure 4, the CH_3OH ($E_{\text{u}} = 45$ K) and H_2CO ($E_{\text{u}} = 21$ K) transitions exhibit tentative components at $\Delta p \sim \pm 1''5$. Given their proximity to the edges of the bipolar outflow, we suspect that these emission components may trace the interaction surface between the bipolar outflow and the ambient quiescent material. This could be similar with the arc-like HCOOH emission pattern in Orion-KL observed by Liu et al. (2002).

These components are expected to have low gas temperatures, given their distance (and fewer received photons consequently) from the central protostar and the non-detection in our data of high-upper-energy transitions such as OCS 100 and 111 K (Figure 4). Between the two potential associations, namely grain sputtering or thermal desorption, we favor the former due to the (expected) low temperature. The absence of high-velocity wings, another signature of associations with shocks, may be attributed to the low SNR. In this picture, these components would possibly exhibit chemical similarities to the chemically rich shocked regions such as L1157-B1 (e.g., Arce et al. 2008), also associated with bow shocks. A more sensitive investigation is necessary to reveal the nature of these components.

5. CONCLUSIONS

Using the ALMA Cycle 6 data from the ALMASOP project and archival ALMA Cycle 3 data, our findings include:

1. In the protostellar core HOPS 87, we discovered two chemically rich and localized regions containing CH_3OH , H_2CO , OCS, ^{13}CS , and H_2S near the bases of the molecular bipolar outflow. The position offsets of these regions are consistent with those of the bipolar outflow as traced by CO and SiO, with the northern (blue-shifted) lobe peaking at a larger position offset Δp than the southern (red-shifted) lobe.
2. These localized chemically rich features are more likely due to shocks driven by jets rather than winds, based on the shapes of the PV diagrams. Under the jet-driven shock scenario, the chemically rich and jet-localized regions are likely the knots often detected in jets.
3. Compared to the counterpart hot corino in HOPS 87, the composition of COMs in the shocked regions appears simpler. We speculate that this simple

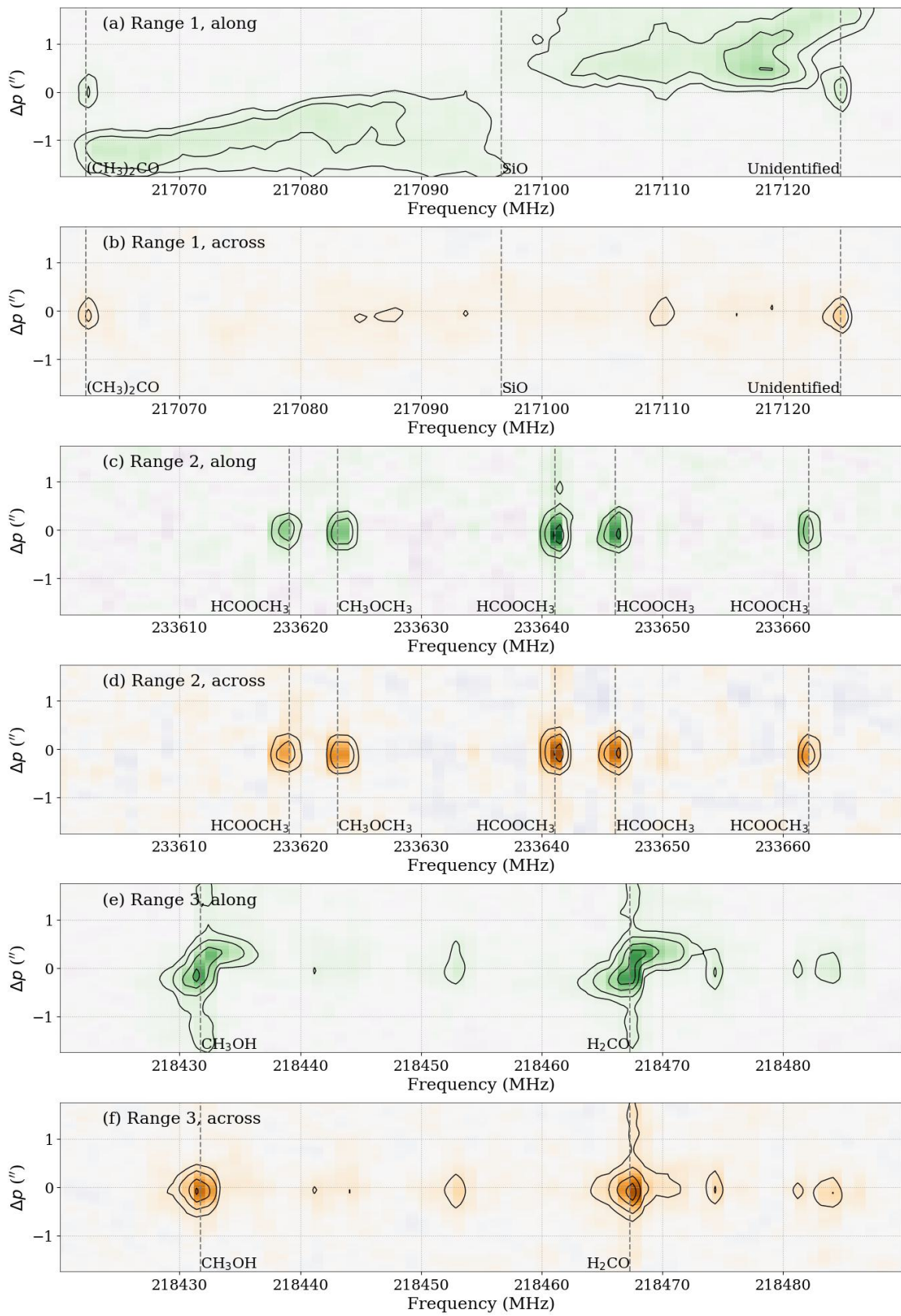


Figure 6. PV diagrams cut along (panels a, c, and e) and across (panels b, d, and f) to the outflow axis for three selected frequency ranges. The x-axes are in terms of frequency. The origin of the y-axes is the continuum peak. The contours represent levels of [10, 20, 30, 40] σ . In panels (a) and (b), the typical outflowing gas tracer, SiO, is visible only in the cut along the outflow axis with a spur structure. Panels (c) and (d) show that COMs like HCOOCH_3 and CH_3OCH_3 display a single peak in both diagrams. In panels (e) and (f), CH_3OH and H_2CO present a single peak in the cut across the outflow axis, accompanied by a two-lobe feature in the cut along the outflow axis.

composition is due to resident dust grains undergoing cycles of ice sublimation and subsequent reformation during their journey from the circumstellar envelope to the jet-localized region. Alternatively, it could result from the shock chemistry, and the chemical composition may further constrain the shock models.

ACKNOWLEDGMENTS

We thank the two anonymous reviewers for valuable comments. This paper makes use of the following ALMA data: ADS/JAO.ALMA#2015.1.00341.S and ADS/JAO.ALMA#2018.1.00302.S. ALMA is a partnership of ESO (representing its member states), NSF (USA) and NINS (Japan), together with NRC (Canada), NSTC and ASIAA (Taiwan), and KASI (Republic of Korea), in cooperation with the Republic of Chile. The Joint ALMA Observatory is operated by ESO, AUI/NRAO and NAOJ. This work made use of Astropy:¹ a community-developed core Python package and an ecosystem of tools and resources for astronomy (Astropy Collaboration et al. 2013; Price-Whelan et al. 2018; Astropy Collaboration et al. 2022). S.-Y. H. and C.-F.L. acknowledge grants from the National Science and Technology Council of Taiwan (110-2112-M-001-021-MY3 and 112-2112-M-001-039-MY3) and the Academia Sinica (Investigator Award AS-IA-108-M01). LB gratefully acknowledges support by the ANID BASALproject FB210003. DJ is supported by NRC Canada and by an NSERC Discovery Grant. Y.-L.Y. acknowledges support from Grant-in-Aid from the Ministry of Education, Culture, Sports, Science, and Technology of Japan (20H05845, 20H05844), and a pioneering project in RIKEN (Evolution of Matter in the Universe).

Software: Astropy (Astropy Collaboration et al. 2013; Price-Whelan et al. 2018; Astropy Collaboration et al. 2022), CASA (CASA Team et al. 2022), CARTA (Comrie et al. 2021),

Table A1. Transitions in this study

Species	E_u (K)	f_{rest} (MHz)	Quantum Number	Database
CO	17	230538	$v=0; J=2-1$	CDMS
SiO	31	217105	$v=0; J=5-4$	CDMS
C ¹⁸ O	16	219560	$v=0; J=2-1$	CDMS
H ₂ CO	21	218222	$J=3-2; K_a=0; K_c=3-2$	CDMS
H ₂ CO	68	218476	$J=3-2; K_a=2; K_c=2-1$	CDMS
H ₂ CO	68	218760	$J=3-2; K_a=2; K_c=1-0$	CDMS
H ₂ CO	174	216569	$J=9; K_a=1; K_c=8-9$	CDMS
CH ₃ OH	45	218440	rovibSym=E; $v=0; J=4-3; K_a=2-1; K_c=3-2$	CDMS
CH ₃ OH	165	232419	rovibSym=A1; $v=0; J=10-9; K_a=2-3; K_c=8-7$	CDMS
CH ₃ OH	190	232945	rovibSym=E; $v=0; J=10-11; K_a=3-2; K_c=7-9$	CDMS
CH ₃ CHO	65	216582	rovibSym=E; $v=0; J=11-10; K_a=1; K_c=10-9$	JPL
HCOOCH ₃	109	216110	rovibSym=E; $v=0; J=19-18; K_a=2; K_c=18-17$	JPL
H ₂ S	84	216710	$v_1=0; v_2=0; v_3=0; J=2; K_a=2-1; K_c=0-1$	CDMS
OCS	100	218903	$J=18-17; v_1=0; v_2=0; v_3=0$	CDMS
OCS	111	231061	$J=19-18; v_1=0; v_2=0; v_3=0$	CDMS
¹³ CS	33	231221	$v=0; J=5-4$	CDMS

NOTE— E_u is the energy of the upper state, f_{rest} is the rest frequency.

APPENDIX

A. MOLECULAR TRANSITIONS

Table A1 shows the molecular transitions used in this study. In addition, Figure A1 shows the integrated intensity maps of the transitions.

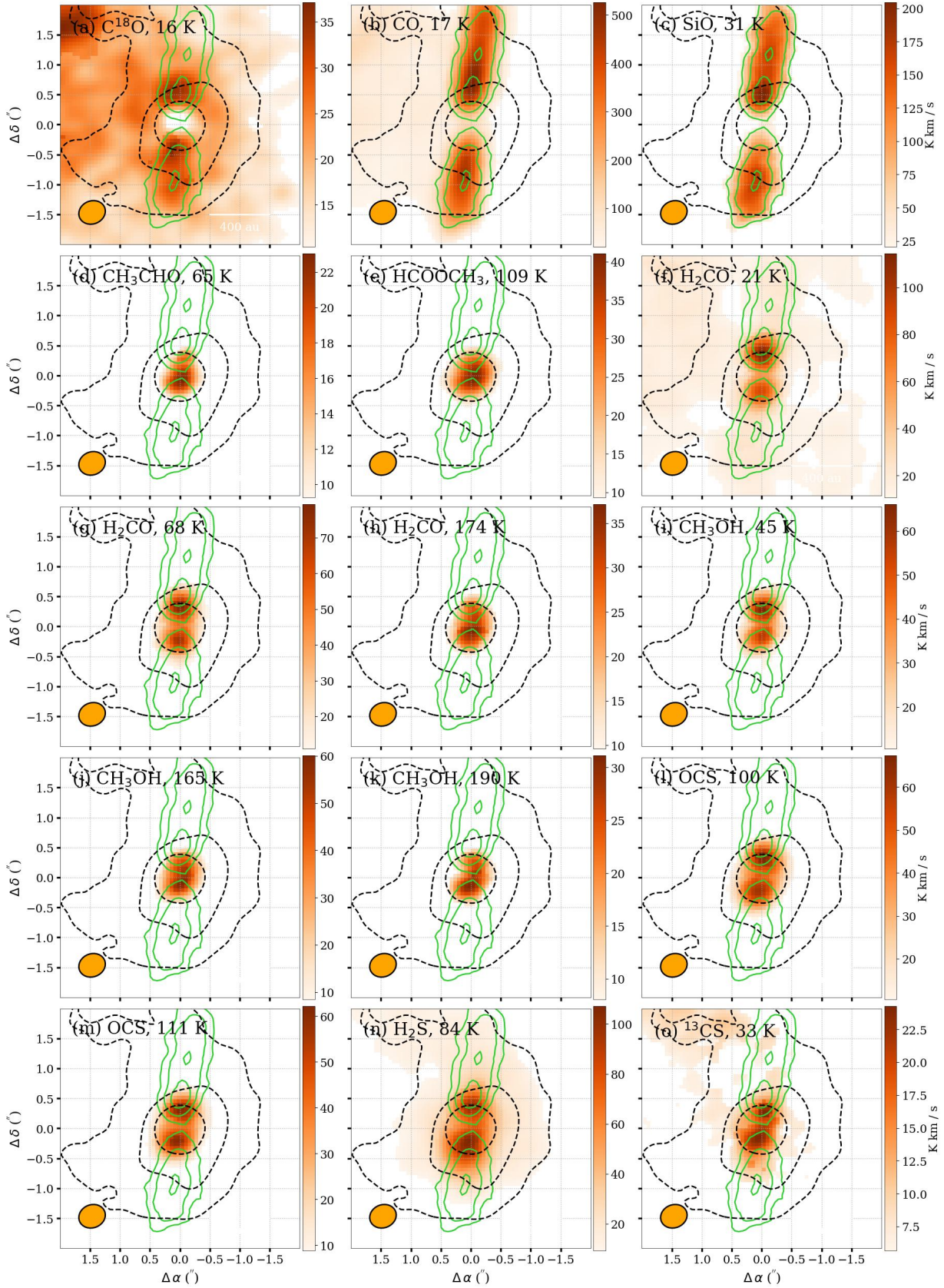


Figure A1. Integrated intensity images of all transitions listed in Table A1. The other captions follow Figure 1. Note that some panels are repeated from Figure 1 but may be labeled differently. The black and the green contours depict the 1.3 mm continuum and the SiO integrated intensity map, respectively.

B. RATIOS BETWEEN PV DIAGRAM

Figure B1 shows the PV diagrams of ratios between flux densities for selected transition pairs.

REFERENCES

- Arce, H. G., Santiago-Garcia, J., Jorgensen, J. K., Tafalla, M., & Bachiller, R. 2008, *Astrophysical Journal Letters*, 681, L21, doi: [10.1086/590110](https://doi.org/10.1086/590110)
- Astropy Collaboration, Robitaille, T. P., Tollerud, E. J., et al. 2013, *A&A*, 558, A33, doi: [10.1051/0004-6361/201322068](https://doi.org/10.1051/0004-6361/201322068)
- Astropy Collaboration, Price-Whelan, A. M., Lim, P. L., et al. 2022, *ApJ*, 935, 167, doi: [10.3847/1538-4357/ac7c74](https://doi.org/10.3847/1538-4357/ac7c74)
- Beckwith, S. V. W., Sargent, A. I., Chini, R. S., & Guesten, R. 1990, *AJ*, 99, 924, doi: [10.1086/115385](https://doi.org/10.1086/115385)
- Benedettini, M., Viti, S., Codella, C., et al. 2021, *A&A*, 645, A91, doi: [10.1051/0004-6361/202039609](https://doi.org/10.1051/0004-6361/202039609)
- Burkhardt, A. M., Shingledecker, C. N., Le Gal, R., et al. 2019, *The Astrophysical Journal*, 881, 32, doi: [10.3847/1538-4357/ab2be8](https://doi.org/10.3847/1538-4357/ab2be8)
- Burkhardt, A. M., Dollhopf, N. M., Corby, J. F., et al. 2016, *The Astrophysical Journal*, 827, 21, doi: [10.3847/0004-637X/827/1/21](https://doi.org/10.3847/0004-637X/827/1/21)
- Busch, L. A., Belloche, A., Garrod, R. T., Müller, H. S. P., & Menten, K. M. 2022, *Astronomy and Astrophysics*, 665, A96, doi: [10.1051/0004-6361/202243383](https://doi.org/10.1051/0004-6361/202243383)
- Busquet, G., Fontani, F., Viti, S., et al. 2017, *Astronomy and Astrophysics*, 604, A20, doi: [10.1051/0004-6361/201730422](https://doi.org/10.1051/0004-6361/201730422)
- CASA Team, Bean, B., Bhatnagar, S., et al. 2022, *Publications of the Astronomical Society of the Pacific*, 134, 114501, doi: [10.1088/1538-3873/ac9642](https://doi.org/10.1088/1538-3873/ac9642)
- Caselli, P., Hartquist, T. W., & Havnes, O. 1997, *Astronomy and Astrophysics*, 322, 296. <https://ui.adsabs.harvard.edu/abs/1997A&A...322..296C>
- Ceccarelli, C. 2004, in *Star Formation in the Interstellar Medium: In Honor of David Hollenbach, Chris McKee and Frank Shu*, ASP Conference Proceeding, ed. D. Johnstone, F. Adams, D. Lin, D. Neufeld, & E. Ostriker, Vol. 323, San Francisco, Astronomical Society of the Pacific (ASP Conference Proceedings)
- Chini, R., Reipurth, B., WardThompson, D., et al. 1997, *Astrophysical Journal*, 474, L135, doi: [10.1086/310436](https://doi.org/10.1086/310436)
- Codella, C., Fontani, F., Ceccarelli, C., et al. 2015, *Monthly Notices of the Royal Astronomical Society*, 449, L11, doi: [10.1093/mnras/lu204](https://doi.org/10.1093/mnras/lu204)
- Codella, C., Ceccarelli, C., Cabrit, S., et al. 2016, *A&A*, 586, L3, doi: [10.1051/0004-6361/201527424](https://doi.org/10.1051/0004-6361/201527424)
- Comrie, A., Wang, K.-S., Hsu, S.-C., et al. 2021, *Astrophysics Source Code Library*, ascl:2103.031. <https://ui.adsabs.harvard.edu/abs/2021ascl.soft03031C>
- Dutta, S., Lee, C.-F., Liu, T., et al. 2020, *ApJS*, 251, 20, doi: [10.3847/1538-4365/abba26](https://doi.org/10.3847/1538-4365/abba26)
- Dutta, S., Lee, C.-F., Johnstone, D., et al. 2024, *The Astronomical Journal*, 167, 72, doi: [10.3847/1538-3881/ad152b](https://doi.org/10.3847/1538-3881/ad152b)
- Feng, S., Codella, C., Ceccarelli, C., et al. 2020, *The Astrophysical Journal*, 896, 37, doi: [10.3847/1538-4357/ab8813](https://doi.org/10.3847/1538-4357/ab8813)
- Furlan, E., Fischer, W. J., Ali, B., et al. 2016, *The Astrophysical Journal Supplement Series*, 224, 5, doi: [10.3847/0067-0049/224/1/5](https://doi.org/10.3847/0067-0049/224/1/5)
- Garrod, R. T., Wakelam, V., & Herbst, E. 2007, *Astronomy and Astrophysics*, 467, 1103, doi: [10.1051/0004-6361:20066704](https://doi.org/10.1051/0004-6361:20066704)
- Guillet, V., Jones, A. P., & Pineau Des Forêts, G. 2009, *Astronomy and Astrophysics*, 497, 145, doi: [10.1051/0004-6361/200811115](https://doi.org/10.1051/0004-6361/200811115)
- Herbst, E., & van Dishoeck, E. F. 2009, *ARA&A*, 47, 427, doi: [10.1146/annurev-astro-082708-101654](https://doi.org/10.1146/annurev-astro-082708-101654)
- Holdship, J., Viti, S., Jiménez-Serra, I., Makrymallis, A., & Priestley, F. 2017, *The Astronomical Journal*, 154, 38, doi: [10.3847/1538-3881/aa773f](https://doi.org/10.3847/1538-3881/aa773f)
- Holdship, J., Jimenez-Serra, I., Viti, S., et al. 2019, *The Astrophysical Journal*, 878, 64, doi: [10.3847/1538-4357/ab1cb5](https://doi.org/10.3847/1538-4357/ab1cb5)
- Hsu, S.-Y., Liu, S.-Y., Liu, T., et al. 2020, *ApJ*, 898, 107, doi: [10.3847/1538-4357/ab9f3a](https://doi.org/10.3847/1538-4357/ab9f3a)
- . 2022, *ApJ*, 927, 218, doi: [10.3847/1538-4357/ac49e0](https://doi.org/10.3847/1538-4357/ac49e0)
- Hsu, S.-Y., Liu, S.-Y., Johnstone, D., et al. 2023, *The Astrophysical Journal*, 956, 120, doi: [10.3847/1538-4357/acefcf](https://doi.org/10.3847/1538-4357/acefcf)
- Izumi, N., Sanhueza, P., Koch, P. M., et al. 2024, *The Astrophysical Journal*, 963, 163, doi: [10.3847/1538-4357/ad18c6](https://doi.org/10.3847/1538-4357/ad18c6)
- James, T. A., Viti, S., Holdship, J., & Jiménez-Serra, I. 2020, *Astronomy and Astrophysics*, 634, A17, doi: [10.1051/0004-6361/201936536](https://doi.org/10.1051/0004-6361/201936536)
- Jiménez-Serra, I., Caselli, P., Martín-Pintado, J., & Hartquist, T. W. 2008, *Astronomy and Astrophysics*, 482, 549, doi: [10.1051/0004-6361:20078054](https://doi.org/10.1051/0004-6361:20078054)
- Juvela, M., He, Jinhua, Pattle, Katherine, et al. 2018, *A&A*, 612, A71, doi: [10.1051/0004-6361/201731921](https://doi.org/10.1051/0004-6361/201731921)
- Kauffmann, J., Bertoldi, F., Bourke, T. L., Evans, N. J., & Lee, C. W. 2008, *A&A*, 487, 993, doi: [10.1051/0004-6361:200809481](https://doi.org/10.1051/0004-6361:200809481)
- Le Gouellec, V. J. M., Greene, T. P., Hillenbrand, L. A., & Yates, Z. 2024, *The Astrophysical Journal*, 966, 91, doi: [10.3847/1538-4357/ad2935](https://doi.org/10.3847/1538-4357/ad2935)
- Lee, C. F., Codella, C., Ceccarelli, C., & Lopez-Sepulcre, A. 2022, *Astrophysical Journal*, 937, 10, doi: [10.3847/1538-4357/ac8c28](https://doi.org/10.3847/1538-4357/ac8c28)
- Lee, C.-F., Codella, C., Li, Z.-Y., & Liu, S.-Y. 2019a, *ApJ*, 876, 63, doi: [10.3847/1538-4357/ab15db](https://doi.org/10.3847/1538-4357/ab15db)

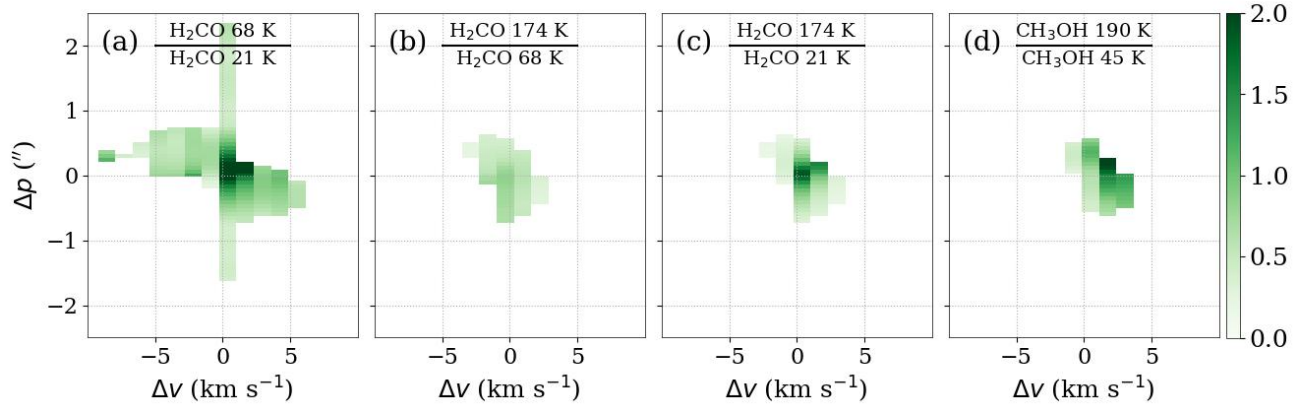


Figure B1. The PV diagrams of ratios between flux densities. The label in each panel denotes the molecular transitions for the numerator and denominator. The pixels having flux density smaller than 5σ are excluded.

- Lee, C.-F., Li, Z.-Y., Ho, P. T. P., et al. 2017, *ApJ*, 843, 27, doi: [10.3847/1538-4357/aa7757](https://doi.org/10.3847/1538-4357/aa7757)
- Lee, C. F., Mundy, L. G., Reipurth, B., Ostriker, E. C., & Stone, J. M. 2000, *Astrophysical Journal*, 542, 925, doi: [10.1086/317056](https://doi.org/10.1086/317056)
- Lee, C.-F., Stone, J. M., Ostriker, E. C., & Mundy, L. G. 2001, *The Astrophysical Journal*, 557, 429, doi: [10.1086/321648](https://doi.org/10.1086/321648)
- Lee, J.-E., Lee, S., Baek, G., et al. 2019b, *Nature Astronomy*, 3, 314, doi: [10.1038/s41550-018-0680-0](https://doi.org/10.1038/s41550-018-0680-0)
- Lefloch, B., Ceccarelli, C., Codella, C., et al. 2017, *Monthly Notices of the Royal Astronomical Society*, 469, L73, doi: [10.1093/mnras/slx050](https://doi.org/10.1093/mnras/slx050)
- Liu, S.-Y., Girart, J. M., Remijan, A., & Snyder, L. E. 2002, *The Astrophysical Journal*, 576, 255, doi: [10.1086/341620](https://doi.org/10.1086/341620)
- Massardi, M., Stoehr, F., Bendo, G. J., et al. 2021, *Publications of the Astronomical Society of the Pacific*, 133, 085001, doi: [10.1088/1538-3873/ac159c](https://doi.org/10.1088/1538-3873/ac159c)
- Mendoza, E., Lefloch, B., Lopez-Sepulcre, A., et al. 2014, *Monthly Notices of the Royal Astronomical Society*, 445, 151, doi: [10.1093/mnras/stu1718](https://doi.org/10.1093/mnras/stu1718)
- Miura, H., Yamamoto, T., Nomura, H., et al. 2017, *The Astrophysical Journal*, 839, 47, doi: [10.3847/1538-4357/aa67df](https://doi.org/10.3847/1538-4357/aa67df)
- Okoda, Y., Oya, Y., Imai, M., et al. 2022, *ApJ*, 935, 136, doi: [10.3847/1538-4357/ac7ff4](https://doi.org/10.3847/1538-4357/ac7ff4)
- Oya, Y., & Yamamoto, S. 2020, *ApJ*, 904, 185, doi: [10.3847/1538-4357/abbe14](https://doi.org/10.3847/1538-4357/abbe14)
- Oya, Y., Moriwaki, K., Onishi, S., et al. 2018, *The Astrophysical Journal*, 854, 96, doi: [10.3847/1538-4357/aaa6c7](https://doi.org/10.3847/1538-4357/aaa6c7)
- Planck, C., Ade, P. A. R., Aghanim, N., et al. 2016, *A&A*, 594, A28, doi: [10.1051/0004-6361/201525819](https://doi.org/10.1051/0004-6361/201525819)
- Price-Whelan, A. M., Sipőcz, B. M., Günther, H. M., et al. 2018, *AJ*, 156, 123, doi: [10.3847/1538-3881/aabc4f](https://doi.org/10.3847/1538-3881/aabc4f)
- Sahu, D., Liu, S. Y., Su, Y. N., et al. 2019, *Astrophysical Journal*, 872, 196, doi: [10.3847/1538-4357/aaffda](https://doi.org/10.3847/1538-4357/aaffda)
- Saito, H., Mizuno, N., Moriguchi, Y., et al. 2001, *Publications of the Astronomical Society of Japan*, 53, 1037, doi: [10.1093/pasj/53.6.1037](https://doi.org/10.1093/pasj/53.6.1037)
- Shang, H., Liu, C.-F., Krasnopolsky, R., & Wang, L.-Y. 2023, *The Astrophysical Journal*, 944, 230, doi: [10.3847/1538-4357/aca763](https://doi.org/10.3847/1538-4357/aca763)
- Shibayama, Y., Watanabe, Y., Oya, Y., et al. 2021, *The Astrophysical Journal*, 918, 32, doi: [10.3847/1538-4357/ac0ef6](https://doi.org/10.3847/1538-4357/ac0ef6)
- Shu, F. H., Shang, H., & Lee, T. 1996, *Science*, 271, 1545, doi: [10.1126/science.271.5255.1545](https://doi.org/10.1126/science.271.5255.1545)
- Spezzano, S., Codella, C., Podio, L., et al. 2020, *A&A*, 640, A74, doi: [10.1051/0004-6361/202037864](https://doi.org/10.1051/0004-6361/202037864)
- Tabone, B., Cabrit, S., Bianchi, E., et al. 2017, *A&A*, 607, L6, doi: [10.1051/0004-6361/201731691](https://doi.org/10.1051/0004-6361/201731691)
- Takahashi, S., & Ho, P. T. P. 2012, *Astrophysical Journal Letters*, 745, L10, doi: [10.1088/2041-8205/745/1/L10](https://doi.org/10.1088/2041-8205/745/1/L10)
- Takahashi, S., Ho, P. T. P., Tang, Y.-W., Kawabe, R., & Saito, M. 2009, *The Astrophysical Journal*, 704, 1459, doi: [10.1088/0004-637X/704/2/1459](https://doi.org/10.1088/0004-637X/704/2/1459)
- Takahashi, S., Machida, M. N., Tomisaka, K., et al. 2019, *Astrophysical Journal*, 872, 70, doi: [10.3847/1538-4357/aaf6ed](https://doi.org/10.3847/1538-4357/aaf6ed)
- Takahashi, S., Saigo, K., Ho, P. T. P., & Tomida, K. 2012, *The Astrophysical Journal*, 752, 10, doi: [10.1088/0004-637x/752/1/10](https://doi.org/10.1088/0004-637x/752/1/10)
- Tychoniec, Ł., van Dishoeck, E. F., van't Hoff, M. L. R., et al. 2021, *A&A*, 655, A65, doi: [10.1051/0004-6361/202140692](https://doi.org/10.1051/0004-6361/202140692)
- Vastel, C., Alves, F., Ceccarelli, C., et al. 2022, *Astronomy and Astrophysics*, 664, A171, doi: [10.1051/0004-6361/202243414](https://doi.org/10.1051/0004-6361/202243414)
- Yamamoto, S. 2016, *Introduction to Astrochemistry: Chemical Evolution from Interstellar Clouds to Star and Planet Formation* (Springer Japan). <https://books.google.com.tw/books?id=Q0sbswEACAAJ>